Disruption avoidance by stabilizing coupled MHD modes using resonant magnetic perturbations on J-TEXT

Ying He[1], Nengchao Wang[1,a], Yonghua Ding[1], Da Li[1], Song Zhou[1], Feiyue Mao[1], Chengshuo Shen[1], Ruo Jia[1], Zhengkang Ren[1], Yuan Gao[1], Zhichao Zhang[1], Shuhao Li[1], Zhuo Huang[1], Haojie Chen[1], Chuanxu Zhao[1], Abba Alhaji Bala[1,2], Wei Zhang[1], Xianli Xie[1], Zhipeng Chen[1], Zhoujun Yang[1], Zhongyong Chen[1], Q. Yu[3], Yuan Pan[1] and J-TEXT team[b]

[1] International Joint Research Laboratory of Magnetic Confinement Fusion and Plasma Physics, State Key Laboratory of Advanced Electromagnetic Engineering and Technology, School of Electrical and Electronic Engineering, Huazhong University of Science and Technology, Wuhan, 430074, China

[2] Physics Department, Federal University Dutse, Jigawa, Nigeria

[3] Max-Planck-Institut für Plasmaphysik, 85748 Garching, Germany

Email: wangnc@hust.edu.cn

Abstract

The coupling of multiple MHD modes can lead to mode locking and major disruption in tokamak plasmas. In the J-TEXT tokamak, the coupling between two small modes, i.e., m/n = 2/1 and 3/1 modes (m and n are poloidal and toroidal mode numbers, respectively), appears when the edge safety factor is reduced to the vicinity of 3. After the mode coupling, the toroidal phase difference between the 2/1 and 3/1 modes equals 0 in the low field side midplane. This phase relation of coupled modes leads to mutual destabilization and even major disruption. A control scheme to avoid disruption caused by coupled modes by resonant magnetic perturbations (RMP) is presented. It is found that the application of RMP significantly changes the evolution of the coupled modes. The coupling of the 2/1 and 3/1 modes occurs earlier as the RMP amplitude increases. The RMP with moderate amplitude can suppress the growth of 2/1 and 3/1 coupled modes and hence avoid disruption. These results provide a possible

[a] Authors to whom any correspondence should be addressed.

[b] See the author list of "N. Wang *et al* 2022 Advances in physics and applications of 3D magnetic perturbations on the J-TEXT tokamak, *Nucl. Fusion* **62** 042016"

strategy for the suppression of neoclassical tearing mode (NTM) seed islands on ITER or future fusion reactors.

1. Introduction

Plasma disruptions pose a serious problem for tokamak progress, limiting the range of operation in plasma current and density. Multiple magnetic islands were observed to correlate with disruptions on many tokamak devices, such as in the density limit discharges of JET[1] and ASDEX Upgrade[2]. The toroidal angular phase velocity of these modes is synchronous[3], i.e., phase-locking with each other. This phenomenon is called mode coupling, which can lead to the flattening of the rotation profile[4,5]. Moreover, the reduction of flow shear has previously been shown to correlate with reduced stability[6,7]. On DIII-D, numerical modeling[8] and experimental observation[9] indicate that the multiple locked magnetic islands produced by error field penetration deteriorate thermal confinement and lead to disruption.

In toroidal plasmas, m/n (m and n are poloidal and toroidal mode numbers, respectively) modes can generate the m/n magnetic perturbation (MP) as well as the $(m \pm 1)/n$ MP due to toroidal coupling ($m/n = 1/0$)[5]. The $(m \pm 1)/n$ MP can (a) directly destabilize the $(m \pm 1)/n$ kink mode, and then evolves to a tearing mode (TM)[3, 10, 11], which is a process similar to the penetration of external applied resonant magnetic perturbations (RMP) or (b) apply an electromagnetic (EM) torque on the $(m \pm 1)/n$ mode and lead to phase locking[5], which is consistent with the interaction between external RMPs and the TM[12,13] or kink mode[14,15]. It is generally assumed that the O-points of coupled modes are toroidally in-phase on the low field side (LFS) mid-plane [5]. Analytical results indicate that such a phase relation of coupled modes will lead to mutual destabilization [5]. It is supported by experimental observations in ASDEX Upgrade [2] and KSTAR [16] that coupled modes can destabilize each other. In addition, external kink modes can also be destabilized by the external MP applied with the same phase, as observed in RFX-mod [17]. These results reveal that one of the coupled modes can produce an external perturbation that destabilizes another kink or tearing mode. With the mutual destabilization of coupled modes, major disruption is usually induced.

Therefore, avoiding the growth of coupled modes is very important for future fusion reactors.

It is shown experimentally that suppressing one of the coupled modes can inhibit the growth of the other mode. In FTU, stabilization of one of the coupled modes by electron cyclotron resonance heating (ECRH) and disruption avoidance has been observed[18]. For the kink mode, a similar process also occurs in EXTRAP T2R, where active feedback stabilization of the resistive wall mode influences the evolution of tearing modes in the central plasma [19]. It is found from previous experimental results that RMP can suppress the small magnetic oscillations (SMOs)[20,21] and the saturated TM with high frequency[22]. It would be attractive to study the impact of RMP on the coupled modes, especially in the initial phase of the coupling.

This work presents the recent observation of mode coupling in J-TEXT when the plasma current keeps increasing (the edge safety factor (q_a) is decreased to the vicinity of 3). Coupling between two small modes, the 2/1 and 3/1 modes, occurs. During mode coupling, both modes grow to a large saturated level and lead to disruption. In the early stages of mode coupling, the structure of coupled modes can be kink or kink-tearing. A control scheme to avoid disruption caused by coupled modes by RMP is presented. It is found that the application of RMP significantly changes the evolution of the coupled modes. Moreover, the paper demonstrates from experiments that the avoidance of disruption was achieved by suppressing the growth of coupled modes. This paper is organized as follows. The experimental setup is introduced in Sec. 2. In Sec. 3, the observation of multiple modes and interaction between multiple modes on the J-TEXT tokamak are shown. The typical results of disruption avoidance by stabilizing coupled modes using RMP are shown in Sec. 4, and the effect of RMP on coupled modes is shown in Sec. 5. Finally, the paper is discussed and summarized in Sec. 6.

2. Experimental setup

J-TEXT[23,24,25] is a conventional medium-sized tokamak with a major radius, R_0, of 1.05 m and a minor radius, a, of 0.25-0.3 m. The typical plasma parameters of a J-TEXT discharge include the toroidal field B_t = 1.2 - 2.2 T, the plasma current

I_p=100 - 230 kA and the central line-averaged electron density n_e= 1-7×10^{19} m^{-3}. The experiments are carried out with ohmically heated plasma in this work.

There are 8 groups of saddle coils installed in the vacuum vessel to produce RMP[26, 27]. In this work, the RMP coils are operated in the m/n = 2/1 dominated mode as used previously in Ref. [20], with a 2/1 RMP of ~1.83 Gauss/kA at 2/1 rational surface and a 3/1 RMP of ~1.35 Gauss/kA at the 3/1 rational surface. The position of the rational surface is calculated by EFIT code with the parameters of discharge 1057567 with q_a ~ 3.1. The MHD activities can be systematically measured by the poloidal and toroidal Mirnov arrays shown in Figure 1 (left)[28,29]. The perturbed poloidal magnetic field (δB_θ) generated by the rotating MHD modes can be obtained by time integration of the Mirnov signal dB/dt and then extracting the high frequency perturbations. The time evolution of δB_θ measured by poloidal and toroidal Mirnov arrays can provide the mode numbers, as will be shown in Figure 2(d1) to (d4). The variation in plasma electron temperature is measured by a heterodyne electron cyclotron emission (ECE) radiometer [30]. Figure 1 (right) shows the radial locations of the ECE channels for the toroidal field of 1.4 T in this work.

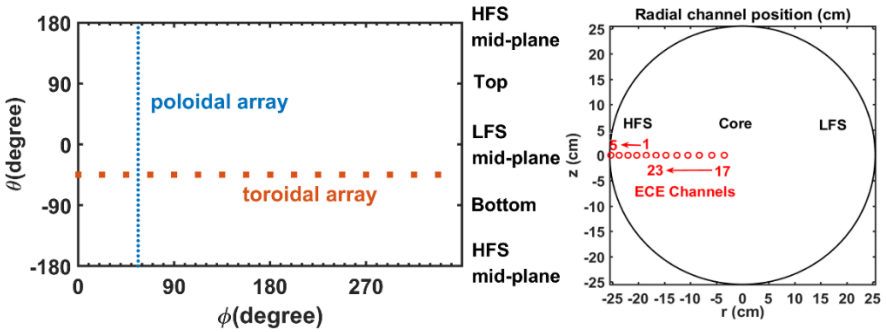

Figure 1 Positions of Mirnov probes[28] and ECE channels at B_t=1.4 T[30].

3. Observation of multiple modes coupling on J-TEXT

3.1 Observation of multiple modes on J-TEXT

In the low beta J-TEXT plasma, the typically observed MHD modes are m/n = 2/1, 3/1 and 1/1 modes. Figure 2 displays one typical example of the coupling process of multiple MHD modes during discharge #1057567. The plasma current I_p is slowly ramped up from 135 kA to ~155 kA. The central line-averaged electron density

n_e= 1.5×10^{19} m^{-3}. The toroidal magnetic field B_t is selected to be 1.4 T so that the edge safety factor q_a is reduced from 3.3 to below 3. In addition, the ECE channels can measure the electron temperature perturbations radially from the plasma boundary to the inside q = 1 rational surface on the high field side (HFS) with high resolution. Such measurement on the LFS is not so feasible: (a) it will need higher B_t and I_p to obtain q_a ~ 3, (b) the spatial resolution of ECE signals is worse in the LFS than that in the HFS due to the smaller radial gradient of the toroidal field.

There is a SMOat ~ 8 kHz since 0.15 s in Figure 2(c). This SMOs is widely observed in J-TEXT discharges without a large saturated 2/1 tearing mode, and its frequency ranges from ~7 kHz to 10 kHz[20]. The mode number of SMOs is m/n = 2/1, as shown in Figure 2(d1). With I_p increasing and q_a decreasing to below 3, a clear magnetic oscillation occurs in the Mirnov signal at 0.33 s (Figure 2(b)). This is due to the appearance of a mode with a frequency at approximately 13 kHz (Figure 2(c)). The time evolution of δB_θ measured by poloidal and toroidal Mirnov arrays indicate that the mode structure is 3/1, as shown in Figure 2(d2). The 3/1 mode should be a kink mode because of q_a < 3. In addition, the 3/1 kink mode frequency decreases from 13 kHz to approximately 11 kHz at 0.4 s, while the 8 kHz component retains its frequency at ~8 kHz.

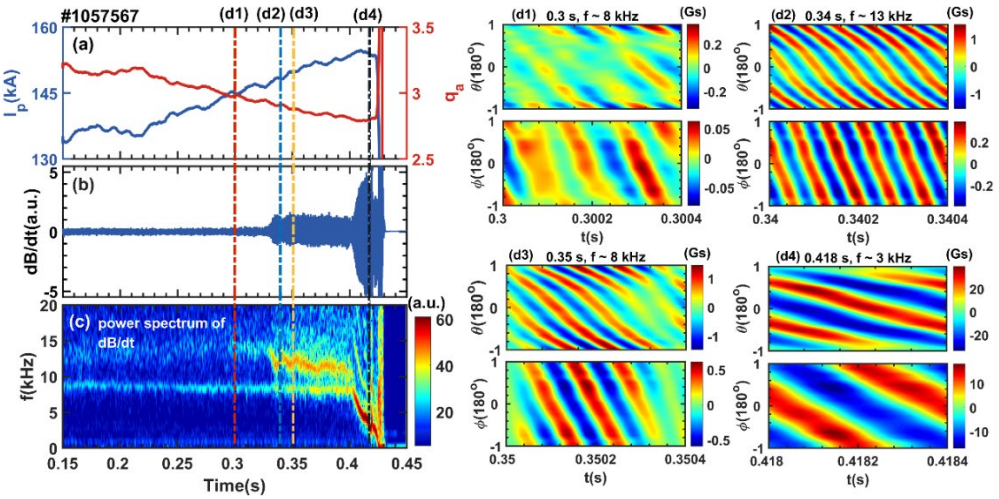

Figure 2 Temporal evolution of (a) the plasma current I_P (blue) and edge safety factor q_a (red), (b) the Mirnov coil signal dB/dt, (c) power spectrum of the Mirnov signal dB/dt, (d1), (d2), (d3) and (d4) the time evolution of the δB_θ measured by the poloidal and toroidal Mirnov probe arrays corresponding to the time indicated by the vertical line in (c), respectively.

Although the 8 kHz mode retains its frequency, its dominant mode number evolves from 2/1 (0.3 s, Figure 2(d1)) to 3/1 (0.35 s, Figure 2(d3)), which means both the 8 kHz mode and the 13 kHz mode have a 3/1 spatial structure. Since the magnetic perturbations are measured outside the plasma, the radial locations of their origination are unclear. Figure 3 reveals essential information of their radial locations via the wavelet power spectrum of ECE signals, which are measured at 6 radial positions covering the $q = 2$ rational surface and plasma boundary (near 3/1 rational surface when $q_a > 3$) around $r \sim$ -19 cm and -25.3 cm, respectively. It is noted that the radial location of 2/1 rational surface, $r_s^{2/1}$, move from -18.9 cm to -19.5 cm during the q_a ramping down from 2.96 to 2.8 (0.3 s to 0.4 s), as estimated by the EFIT equilibrium reconstruction. This outward movement of 0.6 cm is small compared to the spatial resolution of ECE channels, so the effect of $r_s^{2/1}$ variation is neglected. It is found from Figure 3(e) that the 8 kHz oscillation can be observed at r = -18.5 cm from 0.3 s until 0.4 s. This indicates that there is always a 2/1 SMO at 8 kHz. The appearance of the 3/1 kink mode at 0.33 s leads to the 13 kHz electron temperature oscillation at the plasma boundary ($r \sim$ -23.7 cm and -25.3 cm). With the decrease of 3/1 kink mode frequency from 13 kHz to 11 kHz, an 8 kHz component appears in the ECE signal measured at -25.3 cm (Figure 3(*a*)) since 0.35 s. It indicates that a new 3/1 structure at 8 kHz frequency appears together with the 2/1 SMO. It is reasonable to speculate that the 8 kHz 3/1 structure produces larger magnetic perturbations than the 2/1 SMO, so that the magnetic feature of the 8 kHz component is dominant to 3/1 structure after 0.35 s. It will be shown in the following sub-section that the interaction between 2/1 SMO (8 kHz) and 3/1 kink mode (13~11 kHz) can induce non-uniformly rotation of 3/1 kink mode and then produces 8 kHz harmonics with 3/1 spatial structure.

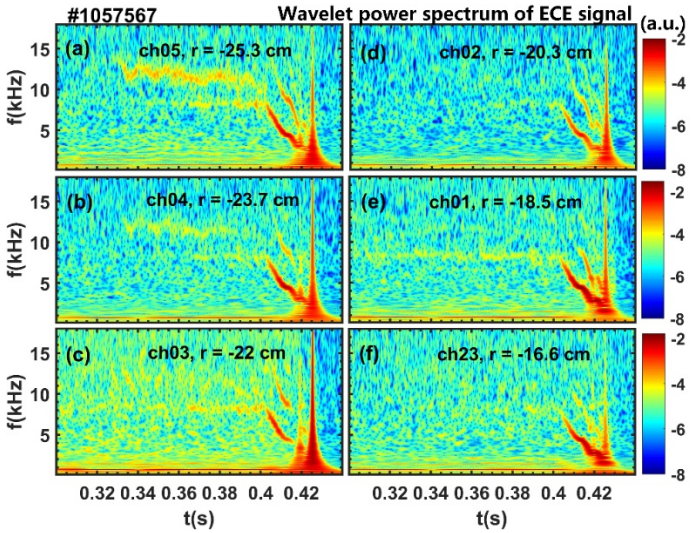

Figure 3 Wavelet power spectrum of ECE signals at (a) -25.3 cm, (b) -23.7 cm, (c) -22 cm, (d) -20.3 cm, (e) -18.5 cm and (f) -16.6 cm.

3.2 Interaction between multiple modes on J-TEXT

Figure 4 (a) and (b) display the power spectral density analysis for the Mirnov signal and the ECE signal from a channel at the plasma boundary at $t = 0.35$ s, respectively. In addition to the peak frequency at $f_0 = f^{3/1} = 11.7$ kHz and $f_L = 8.3$ kHz, there is a third frequency peak at $f_H = 15.1$ kHz. Note that $f_H = 2f_0 - f_L$. At approximately 0.37 s, the frequency of the 3/1 mode and the third frequency decrease to 11.2 kHz and 14.1 kHz, respectively, as shown in Figure 4 (d) and (e). The frequency of this third harmonics actually varies with the other two with $f_H = 2f_0 - f_L$, i.e., $15.1 = 2 \times 11.7 - 8.3$ at 0.35 s and $14.1 = 2 \times 11.2 - 8.3$ at 0.37 s. The bicoherence[31] of Mirnov probes quantifies the extent of correlation between frequency pairs (f_1, f_2). The correlation coefficients between two of the modes with f_0, f_L and f_H are relatively large, as shown in Figure 4 (c) and (f) for 0.35 s and 0.37 s. The fact that the interaction resides between the 3/1 kink mode and the 2/1 SMO explains the components at f_L around the 3/1 rational surface. The interaction can be understood as follows:

(1) Due to the toroidal coupling effect[5], the 2/1 SMO at f_L produces a 3/1 MP at the 3/1 rational surface.

(2) The 3/1 MP applies an electromagnetic (EM) torque on the 3/1 mode in a similar manner as an externally applied 3/1 MP. According to Fitzpatrick's model[32],

the EM torque is expressed as

$$T_{EM} \propto -\sin\left(\xi_{2/1} - \xi_{3/1}\right)$$

The EM torque varies from both its amplitude and sign with the phase difference between the 2/1 and 3/1 modes, $\Delta\xi = \xi_{2/1} - \xi_{3/1}$, which equals the phase difference between the 2/1 and 3/1 modes in the LFS midplane ($\Delta\phi$). The 3/1 mode rotation can be either accelerated or decelerated, and hence,

(3) The EM torque induces a forced phase oscillation of the 3/1 mode at Δf in the 3/1 mode rest frame and leads to the frequency components at $f_L = f_0 - \Delta f$ and $f_H = f_0 + \Delta f$ in the laboratory frame.

Such frequency components at $f_L = f_0 - \Delta f$ and $f_H = f_0 + \Delta f$ have also been confirmed in J-TEXT during the mode locking process to a rotating RMP field[33], with the RMP at f_L = 4 kHz and the tearing mode initially at f_0 = 5 kHz. Similar as the locking of 2/1 TM to rotating 2/1 RMP, the 3/1 mode locks to the 2/1 SMO at 0.4 s in #1057567, i.e., the 3/1 and 2/1 modes become the coupled modes.

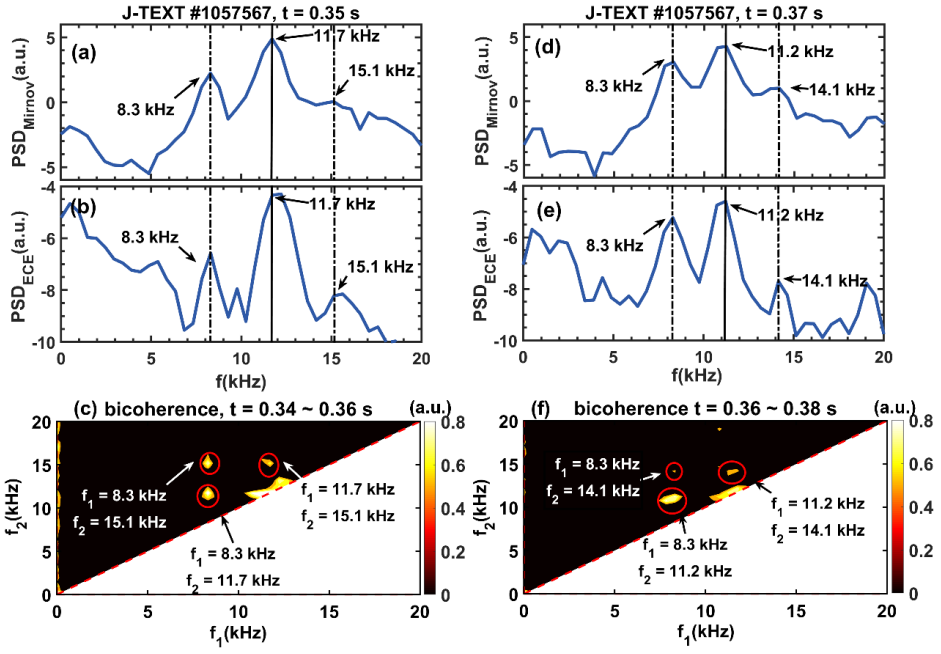

Figure 4 Power spectral density of the (a) Mirnov probe ($\theta = 0^{\circ}$, $\varphi = 56.25^{\circ}$, r = 31.1 cm) and (b) ECE (r = -25.3 cm) at t = 0.35 s. (c) Bicoherence of Mirnov probes from 0.34 s to 0.36 s. (d), (e) and (f) are the same as (a) to (c) but for t = 0.37 s or 0.36 s ~ 0.38 s.

3.3 The evolution of coupled modes and major disruption

When the coupling between 2/1 SMO and 3/1 kink mode occurs, the frequencies

of the two modes change from different to the same. The frequencies becoming the same are easier to identify, so the mode coupling is also referred to as frequency coupling in this work. After frequency locking between the 2/1 and 3/1 modes at 0.4 s, the perturbed poloidal magnetic field, δB_θ, measured by Mirnov probes in the LFS and HFS are asymmetric, as shown in Figure 5 (a) and (b), respectively. Such simultaneous measurements of δB_θ in the LFS and HFS midplane enable the isolation of the 2/1 and 3/1 components produced by the 2/1 and 3/1 modes. The magnetic perturbations generated by the 2/1 and 3/1 modes are expressed as

$$b_{\theta,2/1}=B_{\theta,2/1}\sin\left(2\theta+\varphi+\xi_{2/1}\right) \quad (1)$$

$$b_{\theta,3/1}=B_{\theta,3/1}\sin\left(3\theta+\varphi+\xi_{3/1}\right) \quad (2)$$

where $B_{\theta,m/1}$ is the $m/1$ component of poloidal magnetic field due to the modes. Other modes are very small and can be ignored. Therefore, the δB_θ measured by the LFS and HFS midplane Mirnov probes can be expressed as

$$\delta B_{\theta,\mathrm{LFS}}=b_{\theta,2/1}|_{\theta=0}+b_{\theta,3/1}|_{\theta=0}=B_{\theta,2/1}\sin\left(\varphi+\xi_{2/1}\right)+B_{\theta,3/1}\sin\left(\varphi+\xi_{3/1}\right) \quad (3)$$

$$\delta B_{\theta,\mathrm{HFS}}=b_{\theta,2/1}|_{\theta=\pi}+b_{\theta,3/1}|_{\theta=\pi}=B_{\theta,2/1}\sin\left(\varphi+\xi_{2/1}\right)-B_{\theta,3/1}\sin\left(\varphi+\xi_{3/1}\right) \quad (4)$$

The magnetic perturbations generated by the 2/1 and 3/1 modes on the LFS midplane ($\theta = 0$) can be derived as

$$b_{\theta,2/1}|_{\mathrm{LFS}}=B_{\theta,2/1}\sin\left(\varphi+\xi_{2/1}\right)=(\delta B_{\theta,\mathrm{LFS}}+\delta B_{\theta,\mathrm{HFS}})/2 \quad (5)$$

$$b_{\theta,3/1}|_{\mathrm{LFS}}=B_{\theta,3/1}\sin\left(\varphi+\xi_{3/1}\right)=(\delta B_{\theta,\mathrm{LFS}}-\delta B_{\theta,\mathrm{HFS}})/2 \quad (6)$$

Taking the envelope of $b_{\theta,2/1}|_{\mathrm{LFS}}$ and $b_{\theta,3/1}|_{\mathrm{LFS}}$ gives the time evolution of $B_{\theta,2/1}$ and $B_{\theta,3/1}$ (i.e., the amplitude of the 2/1 and 3/1 modes), as shown in Figure 5 (c). Then, the phase difference between $b_{\theta,2/1}|_{\mathrm{LFS}}$ and $b_{\theta,3/1}|_{\mathrm{LFS}}$ is that of the 2/1 and 3/1 modes ($\Delta\phi$), as shown in Figure 5 (d). From the spectrum of Mirnov signal (Figure 2 (c)), there is a mode with higher frequency than that of 2/1 and 3/1 coupled modes after 0.4 s, which is the second harmonic of the coupled modes. Considering the amplitude of the second harmonic mode is small, its effect is ignored in estimating magnetic perturbations $b_{\theta,2/1|\mathrm{LHS}}$ and $b_{\theta,3/1|\mathrm{LHS}}$ from the Mirnov coil signals.

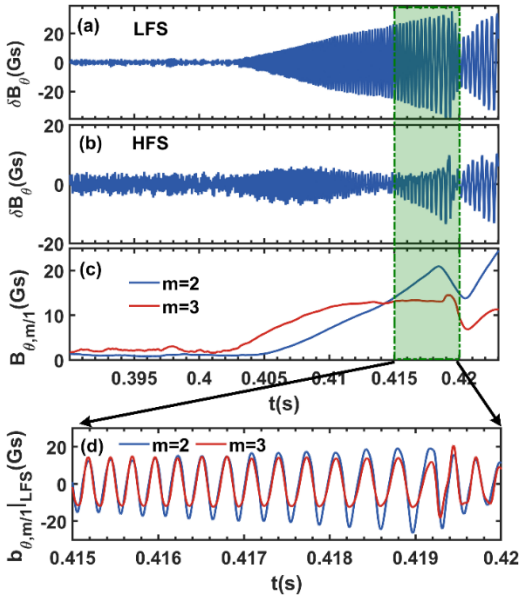

Figure 5 The time evolution of the poloidal magnetic perturbations, δB_θ, of #1057567 measured by the Mirnov probes in the (a) LFS midplane and (b) HFS midplane. (c) The amplitude of the 2/1 and 3/1 modes, and (d) the perturbed b_θ due to 2/1 and 3/1 modes in LFS from 0.415 s to 0.42 s.

The 3/1 and 2/1 amplitudes in Figure 5 (c) show that after frequency coupling, the 3/1 amplitude suddenly grows first, and then the 2/1 mode starts to grow when the amplitude of the 3/1 mode grows to approximately 4.5 Gs at 0.405 s. The 3/1 mode grows to saturation at approximately 13 Gs, and the dominant mode evolves from 3/1 mode to 2/1 mode at approximately 0.414 s. Figure 5 (d) displays $b_{\theta,2/1}|_{\mathrm{LFS}}$ and $b_{\theta,3/1}|_{\mathrm{LFS}}$ from 0.415 s to 0.42 s. This indicates that the phase difference between the 2/1 and 3/1 modes ($\Delta\phi$) equals 0, which is similar to the experimental observation with ohmically heated plasma on ADSEX Upgrade[34]. This phase relation of coupled modes will lead to mutual destabilization or even major disruption [5,17]. The growths of both the 2/1 and 3/1 modes indicate that the coupled modes destabilize each other. With the growth of the 2/1 amplitude above 20 Gs at 0.42 s, a minor collapse occurs, and the amplitudes of the 2/1 and 3/1 modes decrease suddenly. Following the recovery and further growth of mode amplitudes, the major disruption occurs at approximately 0.425 s.

The above experimental results indicate that the coupled 2/1 and 3/1 modes can destabilize each other and lead to disruption. It might be easier to control when the amplitudes of the 2/1 and 3/1 modes are very small before coupling. This paper proposes to suppress these small modes by RMP, which will be presented in next section.

4. Disruption avoidance by stabilizing coupled modes using RMPs

In this section, a control scheme to avoid the disruption by suppressing the growth of coupled modes using RMP is presented. Figure 6 displays the effect of static RMPs with different amplitudes on the mode coupling of the 2/1 and 3/1 modes. The RMP coil current (I_{RMP}) is applied when there are SMOs with high frequency. A small RMP coil current, I_{RMP} = 1 kA, advances the mode coupling and disruption for approximately 0.04 s in shot 1057572 (red) compared to the case without RMPs in shot 1057567 (blue). The earlier mode coupling with RMP will be discussed and explained in detail in Figure 12. When a larger amplitude of static RMP is applied for shot 1057582 (green) with I_{RMP} = 1.5 kA, the plasma current keeps increasing until the end of discharge without large 2/1 and 3/1 modes and disruption. For discharge 1057585 (yellow) with I_{RMP} = 2.5 kA, the 2/1 RMP penetration occurs [35], as identified by the sharp increase of plasma rotation, the disappearance of the sawtooth oscillation and the reduction of electron density. Following RMP penetration, a major disruption occurs at 0.323 s.

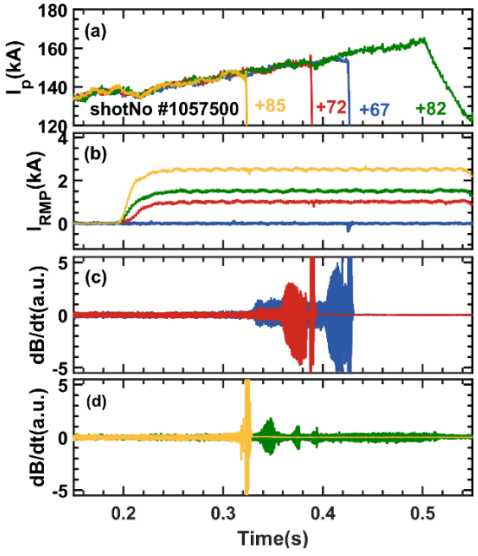

Figure 6 Influence of RMPs with different amplitudes on the disruption caused by mode coupling. Temporal evolution of (a) the plasma current I_p, (b) the RMP coil current I_{RMP}, (c) and (d) the Mirnov signal dB/dt.

Systematic experiments have been carried out by keeping the background plasma parameters the same, while only the amplitude of static RMPs is changed by scanning I_{RMP} from 1 kA to 3 kA. Figure 7 shows the dependence of the maximum I_P reached in the experiments on the RMP amplitude. The blue circle represents discharge without

applying RMP as a reference. For $I_{\mathrm{RMP}} \leq 1.2$ kA, both the maximum I_{P} is reduced, and the disruption time is advanced, as shown by the red open circles. When the amplitude of the RMP coil current increases to the range of 1.5-1.7 kA, disruption can be avoided by suppressing the growth of the coupled modes, as shown by the green squares.

However, stronger RMP lead to 2/1 RMP penetration and major disruption, as shown by the yellow diamonds. So the RMP penetration sets an upper boundary to the disruption avoidance, $I_{\mathrm{RMP,u}}$. In this high RMP amplitude region, the coupled modes can be successfully suppressed, if the penetration doesn't occur before the appearance of mode coupling. Generally, the RMP penetration threshold decreases with increasing I_{p} (corresponding to decreasing q_{a}). With fixed RMP amplitude being larger than $I_{\mathrm{RMP,u}}$, the penetration threshold can reduce with the increasing I_{P} to below the applied RMP amplitude and hence the locked island is induced and lead to disruption. With larger I_{RMP}, this condition is met earlier and hence the maximal I_{p} is smaller, as shown by the yellow diamonds in Figure 7 with I_{RMP} increasing from 2 kA to 3 kA. It is noted that the maximal I_{p} can be slightly larger than the reference case (blue dot) if I_{RMP} is slightly larger than $I_{\mathrm{RMP,u}}$, such as the case with I_{RMP} = 2 kA in Figure 7.

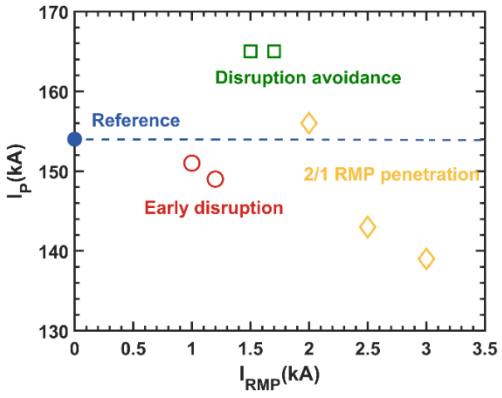

Figure 7 The dependence of maximum I_{p} reached in experiments on RMP amplitude. Blue solid circle: reference ($I_{\mathrm{RMP}} = 0\ kA$), red open circle: early disruption ($I_{\mathrm{RMP}} \leq 1.2$kA), green squares: disruption avoidance ($I_{\mathrm{RMP}} = 1.5 - 1.7\ kA$), yellow diamonds: 2/1 RMP penetration ($I_{\mathrm{RMP}} \geq 2$ kA)

To further confirm the effect of the RMPs on the mode coupling, the RMP with a moderate amplitude is removed in advance compared to #1057582, as shown in Figure 8. During the application of RMP with I_{RMP}=1.7 kA, there is an 8 kHz magnetic fluctuation at approximately 0.33 s. The phase differences of δB_{θ} measured by the poloidal and toroidal Mirnov arrays indicate that the structure of the magnetic

fluctuation is 3/1 (Figure 8 (d1)). It will be shown later in Figure 10 and Figure 11 that this is actually the co-existence of 3/1 kink mode and 2/1 SMO in the frequency coupling status. While as a comparison for the case without RMP, the 3/1 kink mode and 2/1 SMO are not coupled at 0.35 s in Figure 2. Then it is suppressed without reappearance, as shown in Figure 8 (e). However, once the RMP is removed at 0.45 s, the fast growth of the 2/1 and 3/1 modes follows. The 2/1 mode starts to grow rapidly when the amplitude of the 3/1 mode increases to approximately 4 Gs. Then, followed by the saturation of $B_{\theta,3/1}$ at ~12 Gs, the 2/1 mode grows and becomes the dominant mode at approximately 0.43 s. These experimental results indicate that the RMPs with moderate amplitude can suppress the growth of small 2/1 and 3/1 modes.

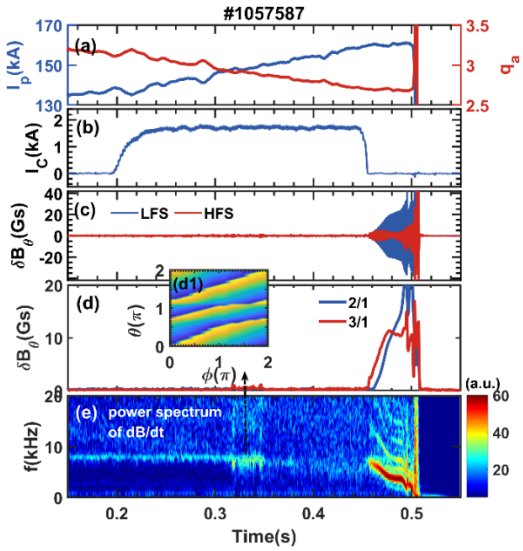

Figure 8 Temporal evolution of (a) the plasma current I_p (blue) and safety factor q_a (red). (b) The current of RMP coil I_{RMP}. (c) The time evolution of δB_θ of #1057587 measured by the Mirnov probes in the LFS midplane (blue) and HFS midplane (red). (d) The amplitude of 2/1 (blue) and 3/1 mode (red). (e) Power spectrum of the Mirnov signal dB/dt. (d1) The phase differences of δB_θ measured by the poloidal and toroidal Mirnov arrays at 0.33 s.

5. The effect of RMPs on coupled modes

5.1 The effect of RMPs on the evolution of coupled modes

To understand how the disruption is avoided with moderate RMP, it is noted that several small bursts of MHD modes emerge, as indicated by the green curve for discharge 1057582 in Figure 6 (d). The first burst appears at 0.335 s, which is at a similar time and I_p as the appearance of the 3/1 mode in the case without RMP (blue, #1057567). However, with a moderate RMP, the modes vanish shortly after the

appearance. Figure 9 displays the detailed evolution of the modes in this discharge with (c) and (d) the poloidal magnetic perturbation δB_θ measured by the Mirnov probes in the LFS midplane and HFS midplane respectively, (e) the power spectrum of the Mirnov signal in the LFS midplane. It is observed from the power spectrum of the Mirnov signal in the LFS midplane that these bursts of modes appear at approximately 6 kHz together with their higher harmonics (Figure 9 (e)). The δB_θ measured from the LFS and HFS display clear poloidal asymmetry. These features indicate that these bursts could be due to the coupled 2/1 and 3/1 modes.

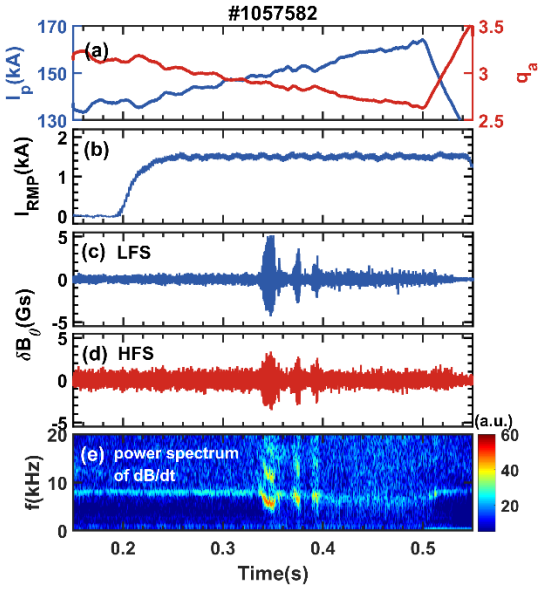

Figure 9 Temporal evolution of (a) the plasma current I_p (blue) and safety factor q_a (red). (b) The current of RMP coil I_RMP. (c) and (d) The poloidal magnetic perturbation δB_θ in the LFS midplane and HFS midplane, respectively. (e) Power spectrum of the Mirnov signal in the LFS midplane to show the mode frequency and amplitude.

Applying the analysis described in the previous section, δB_θ, shown in Figure 9 (c) and (d), can be decomposed into the contributions from the coupled 2/1 and 3/1 modes, as shown in Figure 10 (a) and (e). For each burst, the 3/1 mode grows fast with decreasing frequency and vanishes at a faster rate with a slight recovery of its frequency, which is similar to the RMP suppressing the TMs with high frequency [22]. The 3/1 mode subsequently grows to a smaller amplitude. Along with the growth of the 3/1 mode, the 2/1 mode shows similar evolutions but a smaller amplitude, and it can hardly be observed during the third burst at 0.39 s. Figure 10 (b) to (d) and (f) to (h) show the spectrum of the ECE signals measured from r = -25.3 cm to -16.6 cm, covering from the plasma boundary to inside the 2/1 rational surface. The modes observed from the

ECE signal spectra at -25.3 cm (Figure 10(b)) and -18.5 cm (Figure 10(g)) resemble the amplitude evolution of the 3/1 and 2/1 modes, respectively. Considering that q_a is slightly smaller than 3 and the 2/1 rational surface is located at ~ 18.5 cm, it is considered that the 3/1 mode contributes to the ECE perturbation δI_{ECE} in Figure 10(b) and that the 2/1 mode leads to δI_{ECE} in Figure 10(g). There is no δI_{ECE} at -20.3 cm (Figure 10(f)), and δI_{ECE} at -22 cm and -23.7 cm decrease and disappear with the smaller amplitude of 3/1 during the latter two bursts. This is also shown by the radial profile of the relative perturbation amplitude $\delta I_{ECE}/\langle I_{ECE}\rangle$ in Figure 10(i).

In summary, the experimental results are that (*a*) the 3/1 mode being an external kink mode couples with the 2/1 mode, (*b*) then they grow to a small saturated value followed by a fast decay where the RMPs should play a role, and (*c*) the saturated value is smaller with the decrease in q_a.

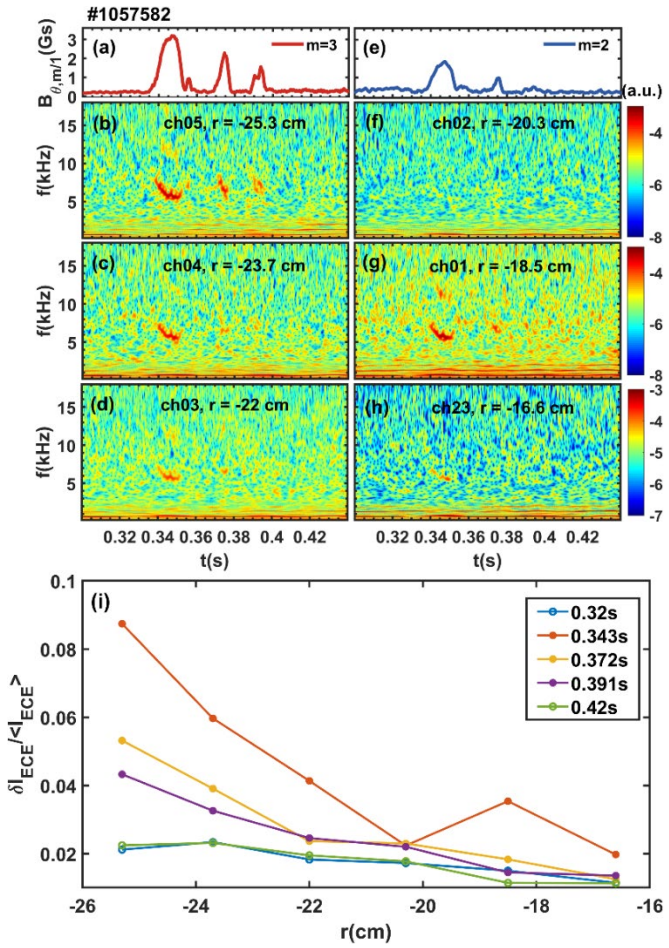

Figure 10 (a) and (e) The amplitude B_θ of the 3/1 and 2/1 modes, respectively. Wavelet power spectrum of the ECE signal at (b) -25.3 cm, (c) -23.7 cm, (d) -22 cm, (f) -20.3 cm, (g) -18.5 cm and (h) -16.6 cm, respectively. (i) Radial profile of $\delta I_{ECE}/\langle I_{ECE}\rangle$ at different times.

Figure 11 displays further details on how the RMP influences the evolution of coupled modes, and t_c is the time of frequency coupling between the 2/1 and 3/1 modes. Figure 11 (a) and (b) compare the time evolution of the 3/1 and 2/1 mode amplitudes for various RMP amplitudes. With the increase in RMP amplitude, the 3/1 and 2/1 modes grow slower to a lower saturated value, and with RMP being above 1.5 kA, the coupled modes transition to a new status of mode suppression. In addition, with the increase in RMP amplitude, the onset of mode frequency coupling appears earlier and at smaller I_{p}, as shown in Figure 12. This reflects that the RMP braking effects on the modes increase with the RMP amplitude. This might be caused by the 3/1 RMP reducing the 3/1 mode frequency and leading to coupling.

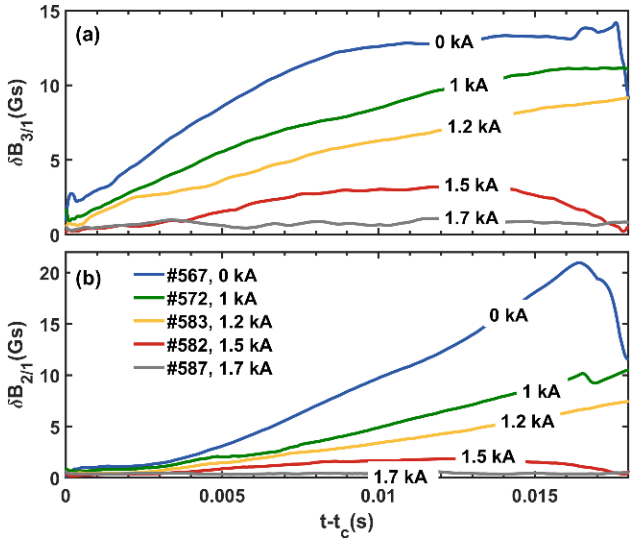

Figure 11. The effect of amplitude of RMPs on the evolution of (a) 3/1 and (b) 2/1 modes amplitudes after mode frequency coupling, t_c is the time of mode frequency coupling. Blue line: I_{RMP}=0 kA, green line: I_{RMP}=1 kA, yellow line: I_{RMP}=1.2 kA, red line: I_{RMP}=1.5 kA and gray line: I_{RMP}=1.7 kA.

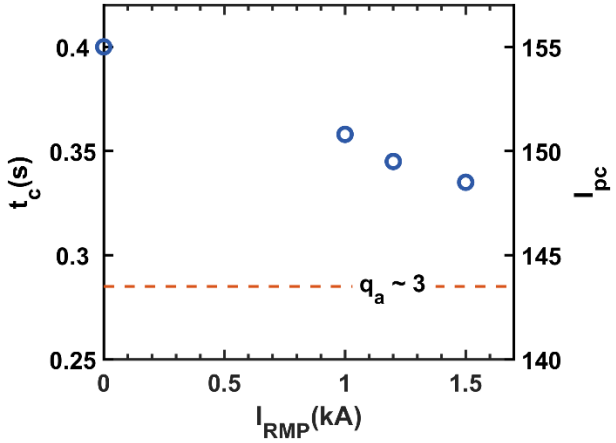

Figure 12. The dependence of the time t_{c} and plasma current I_{pc} of frequency coupling on RMP amplitude.

5.2 The effect of q_a on the evolution of coupled mode

To further study the role of the 3/1 mode in the coupling process, the evolution of coupled modes is studied in this subsection.

The RMP with I_{RMP}=1.7 kA is applied during the q_a ramp down and then removed at different q_a values in a similar manner as in Figure 8. Figure 13 displays the effect of q_a on the evolution of coupled modes. In the reference discharge without RMP (#1057567, Figure 2), the coupling of the 2/1 and 3/1 modes occurs at $q_a \sim 2.8$. The RMP is applied and removed at $q_a \sim 2.8$ (#1057586) and $q_a \sim 2.7$ (#1057587), respectively. Figure 13 shows the evolution of coupled modes amplitude and poloidal magnetic perturbation amplitude change rate of the 2/1 mode, $A'_{2/1} = \mathrm{d}(B_{\theta,2/1})/\mathrm{d}t$, and that of the 3/1 mode, $A'_{3/1} = \mathrm{d}(B_{\theta,3/1})/\mathrm{d}t$, at different q_a, where the the $B_{\theta,2/1}$ and $B_{\theta,3/1}$ are the amplitude of 2/1 and 3/1 mode in equation (1) and (2). Compared to the natural coupling of the 2/1 and 3/1 modes without RMP at $q_a \sim 2.8$ (red line), the amplitude of the 3/1 modes with RMP removal at $q_a \sim 2.8$ (yellow line) is smaller (Figure 13 (b)). This is caused by the suppression of 3/1 mode by RMP, as shown in Figure 8. However, $B_{\theta,3/1}$ has a similar change rate when the occurrence of the coupled mode at $q_a \sim 2.8$ with or without RMP (Figure 13 (d)). After removing RMP at $q_a \sim 2.7$, the change rate of $B_{\theta,3/1}$ is smaller than that of $q_a \sim 2.8$. This indicates that the evolution of the 3/1 mode is sensitive to q_a, and the 3/1 mode is more unstable when 3 - q_a is smaller. From Figure 13 (a) and (c), the evolution of the 2/1 mode has no direct correlation with q_a. Figure 14 displays the change rate of $B_{\theta,2/1}$ on the 3/1 mode amplitude at $q_a \sim 2.8$ and $q_a \sim 2.7$. It is found that the evolution of the 2/1 mode is barely sensitive to q_a. However, $A'_{2/1}$ is proportional to the amplitude of 3/1. The results indicate that the 3/1 mode destabilizes the 2/1 mode after mode coupling.

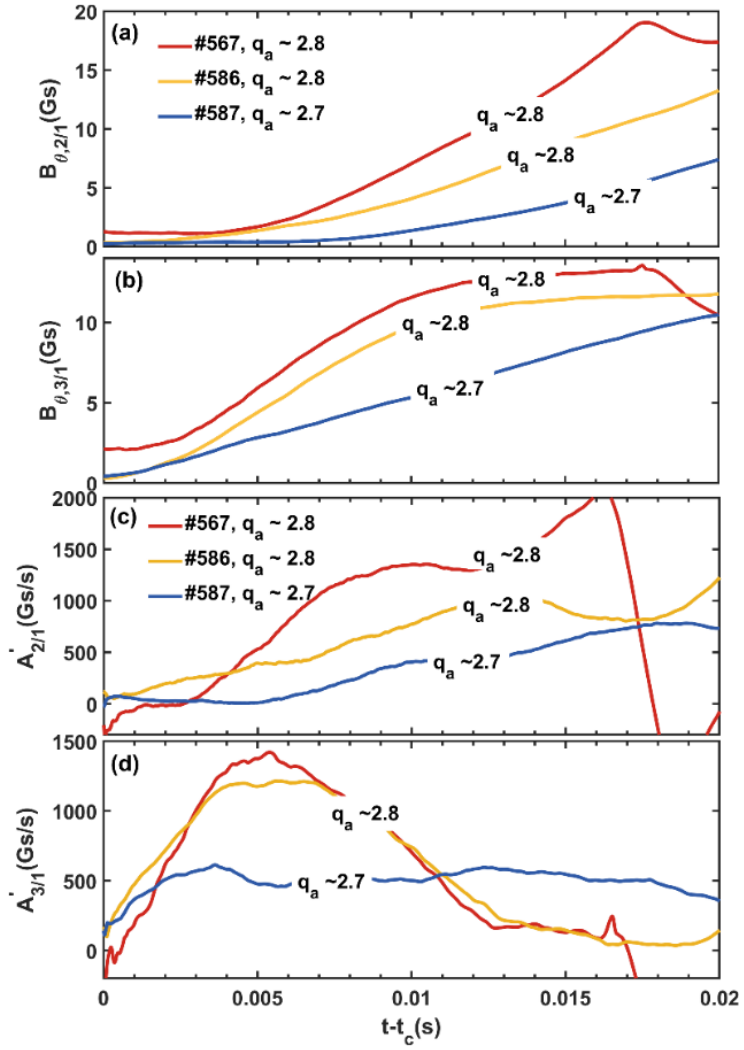

Figure 13 The evolution of (a) 2/1 and (b) 3/1 coupled modes amplitudes at different q_a. The changes rate of the 2/1 mode amplitude, $A'_{2/1} = \mathrm{d}(B_{\theta,2/1})/\mathrm{d}t$, and (d) that of the 3/1 mode amplitude, $A'_{3/1} = \mathrm{d}(B_{\theta,3/1})/\mathrm{d}t$, at different q_a. Red line: #1057567, without RMP. Yellow line: #1057586, removal of RMP at q_a~2.8. Blue line: #1057587, removal of RMP at q_a~2.7.

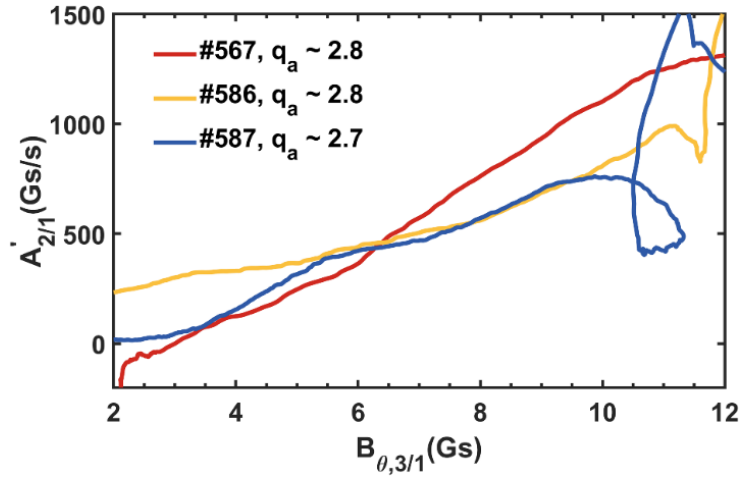

Figure 14 Dependence of the change rate of the 2/1 mode amplitude, $A'_{2/1} = \mathrm{d}(B_{\theta,2/1})/\mathrm{d}t$, on the 3/1 mode amplitude at different q_a.

5.3 Discussion on the mechanism of the impact of RMP on the coupled modes

Figure 15 displays the dependence of the 2/1 mode amplitude, $B_{\theta,2/1}$, and the phase difference between the 2/1 and 3/1 modes in the LFS midplane, $\Delta\phi$, on the 3/1 mode amplitude with various RMP amplitudes. As the RMP amplitude increases, the phase difference between the two modes evolves more quickly toward 0, i.e., in-phase. This final state of $\Delta\phi \sim 0$ may be related to the fact that the 2/1 and 3/1 components of the RMPs are almost in phase in the LFS mid-plane. For $I_{\mathrm{RMP}} = 1.2\ kA$, the 2/1 mode amplitude grows faster when $\Delta\phi$ equals 0°, and $B_{\theta,3/1}$ grows to ~ 2.5 Gs. As a comparison for the case with $I_{\mathrm{RMP}} = 0\ kA$, the amplitude of the 2/1 mode starts to grow when $\Delta\phi$ equals 70° and the 3/1 mode amplitude is 4.5 Gs (Figure 16 (a)). These results suggest that the growth of 2/1 can be influenced by both $\Delta\phi$ and the amplitude of the 3/1 mode. For $I_{\mathrm{RMP}} = 1.5\ kA$, the 2/1 and 3/1 mode amplitudes evolve to approximately 1.65 Gs and 3.3 Gs, respectively. However, for $I_{\mathrm{RMP}} = 1.5\ kA$, the reason why the 2/1 amplitude grows quickly when the 3/1 amplitude is very small is not yet clear.

Figure 16 is the expanded view of Figure 15(a) for the case with $I_{\mathrm{RMP}} = 1.5\ kA$. Following the time evolution shown by the arrows, the 2/1 mode amplitude reduces by more than 5% at the maximal $B_{\theta,3/1}$, and then the simultaneous reductions of $B_{\theta,2/1}$ and $B_{\theta,3/1}$ follow. It is noted that the RMP has been previously applied to suppress small magnetic oscillations [20,21] and high-frequency saturated TMs[22]. The advance of the 2/1 mode suppression compared to that of the 3/1 mode leads to the speculation that the 2/1 RMP field suppresses the growth of the 2/1 mode, and the growth of the 3/1 mode also holds back. The suppression of the 2/1 mode may then affect the evolution of the 3/1 mode. In FTU, stabilization of one of the coupled modes by ECRH and disruption avoidance has been observed[18]. However, the current experimental evidence is not conclusive, especially because the advance time is small.

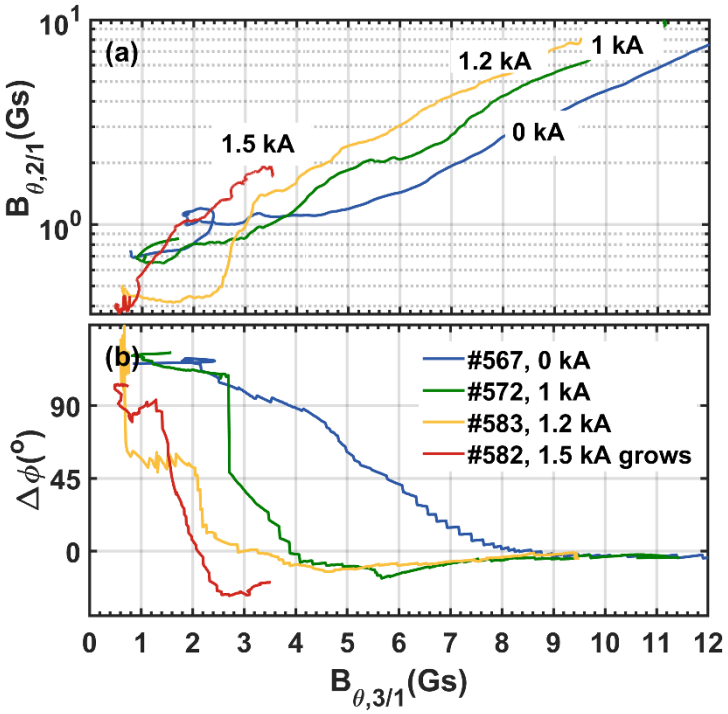

Figure 15 (a) The evolutionary relationship between the 3/1 and 2/1 mode amplitudes after mode coupling with the application of RMPs. Blue line: $I_{\mathrm{RMP}} = 0\ kA$, green line: $I_{\mathrm{RMP}} = 1\ kA$, yellow line: $I_{\mathrm{RMP}} = 1.2\ kA$, red line: $I_{\mathrm{RMP}} = 1.5\ kA$ for growing, respectively. (b) The phase difference $\Delta\phi$ between the 2/1 and 3/1 modes with the application of different amplitude RMPs.

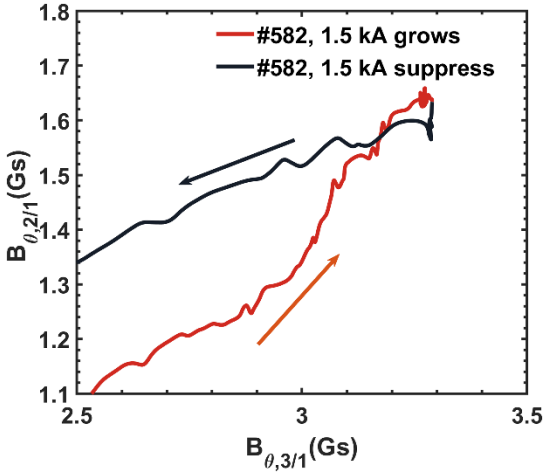

Figure 16 Expanded view of the amplitude evolutionary relationship between the 2/1 and 3/1 modes for $I_{\mathrm{RMP}} = 1.5\ kA$.

The results above indicate that the presence of the external RMP fields with proper amplitude suppresses the coupled 3/1 and 2/1 modes. The underlying mechanism of the impact of RMP on coupled modes is considered to be related to three effects. (1) The 3/1 and 2/1 modes being in-phase in the LFS midplane leads to mutual destabilization of the two modes; (2) the RMP field contributes to the braking of the mode because of the 3/1 component decelerating the 3/1 mode; (3) the RMP contributes to the

suppression effect on either the 3/1 or 2/1 mode, which has a high frequency. The competition leads to either the braking and growth of the coupled modes or the braking and suppression of the modes. It is difficult to distinguish the contributions from those effects based on the current experimental results. Further experimental attempts with a pure 2/1 RMP to control the coupled modes may advance this understanding and will be left for future research.

6. Conclusion and Discussion

In conclusion, this work studies the process of coupling between 2/1 and 3/1 modes and the effect of RMP on the evolution of coupled modes. The phase difference between the 2/1 and 3/1 modes ($\Delta\phi$) equals 0 after phase locking. This phase relation of 2/1 and 3/1 coupled modes leads to mutual destabilization or even major disruption. The experimental results in this paper show that the evolution of the 3/1 mode is sensitive to q_a, and the 3/1 mode is more unstable when $3 - q_a$ is smaller. The growth of the 2/1 mode may be influenced by the phase difference between 2/1 and 3/1 and the magnitude of 3/1. This indicates that the stability of the 3/1 mode has a significant effect on the evolution of the two modes. In addition, a control scheme to avoid disruption caused by coupled modes by RMPs is presented. It is found that the application of RMP significantly changes the evolution of the coupled modes. The coupling of the 2/1 and 3/1 modes occurs earlier as the RMP amplitude increases. The RMP with moderate amplitude can suppress the growth of 2/1 and 3/1 coupled modes and hence avoid disruption.

This paper provides a detailed study of the coupling between 2/1 and 3/1 modes and an in-depth study of the influence of RMP on the coupled modes in J-TEXT, which is helpful to understand the process and control methods of mode coupling. The electromagnetic (EM) torque between the 2/1 and 3/1 modes with different frequencies is similar to the interaction between RMP and the tearing mode[12,13] or kink mode[14,15], which can lead to phase locking. This work shows that the phase difference between the 2/1 and 3/1 modes ($\Delta\phi$) equals 0 after phase locking (Figure 5 (d)), which is similar to the experimental observation with ohmically heated plasma on ADSEX Upgrade[34].

In addition, after frequency coupling, the 3/1 mode grows first, and then the 2/1 mode starts to grow when the amplitude of the 3/1 mode grows to approximately 4.5 Gs without RMP. The change rate of the 2/1 mode amplitude is proportional to the amplitude of 3/1 mode (Figure 14). The growths of both the 2/1 and 3/1 modes indicate that the coupled modes destabilize each other and then lead to disruption, which confirms the previous theory [5]. Therefore, the avoidance of mode coupling and the control of the coupled modes will be important to avoid disruption for future reactor devices.

In addition, this paper proposes a control scheme to suppress the growth of the coupled modes by RMP. The paper demonstrates experimentally that the avoidance of disruption can be achieved by suppressing the growth of coupled modes, which can provide a reference for future devices to avoid disruption due to coupled modes. The mechanism on how the RMP impacts the coupled modes has been discussed in Section 5.3. However, both the 2/1 and 3/1 RMPs could influence the evolution of individual modes, and the RMP coils are operated with the similar amplitudes of 2/1 and 3/1 components. This situation poses an obstacle on distinguishing the roles of either 2/1 or 3/1 RMP. And the phase of the RMP and the relative phase between 2/1 and 3/1 RMP components were not adjust in these experiments. The intrinsic error field (EF) on J-TEXT is about 0.6 Gs[36] . Considering that the RMP current involved in this paper is small, the effect of EF may not be ignored. When the RMP phase is adjusted, the RMP current interval corresponding to the disruption avoidance may change. Further experimental attempts with pure 2/1 RMP or pure 3/1 RMP on controlling the coupled modes and adjusting the phase difference between 2/1 and 3/1 RMP component[37] will support the understanding of the evolution of coupled modes, and it will be left for future research.

In the high-performance tokamak plasma, the coupled modes usually involve the neoclassical tearing modes (NTMs), which evolves from seed magnetic islands. Recent experiments on DIII-D show that 2/1 NTM seed island can be excited by three-wave interaction between coupled modes. In the stage of seed island, the island amplitude is small and the island frequency is high. Compared to the large TM, it is easier to suppress

the smaller modes by RMPs. The strategy proposed in this paper may be used to suppress the evolution of seed islands or the coupled modes which drive the seed islands, and hence avoiding major disruption on ITER or future fusion reactors.

Acknowledgments

The authors are very grateful for the help of the J-TEXT team. This work is supported by the National MCF Energy R&D Program of China under Grant No. 2019YFE03010004, the National Natural Science Foundation of China (Contract No. 12075096, No. 12047526, No. 11905078 and No. 51821005) and "the Fundamental Research Funds for the Central Universities" under Grant No. 2020kfyXJJS003.

References

[1] J. A. Wesson *et al* 1989 *Nucl. Fusion* 29 641
[2] W. Suttrop *et al* 1997 *Nucl. Fusion* 37 119
[3] B. Tobias *et al* 2016 *Phys. Plasmas* 23 056107
[4] C. C. Hegna *et al* 1999 *Phys. Plasmas* 6 130
[5] R. Fitzpatrick *et al* 2015 *Phys. Plasmas* 22 042514
[6] P. Politzer *et al* 2008 *Nucl. Fusion* 48 075001
[7] R. La Haye *et al* 2010 *Phys. Plasmas* 17 056110
[8] Q. Hu *et al* 2019 *Nucl. Fusion* 59 016005
[9] X. D. Du *et al* 2019 *Phys. Plasmas* 26 042505
[10] V. Igochine *et al* 2014 *Phys. Plasmas* 21 110702
[11] V. Igochine *et al* 2019 *Nucl. Fusion* 59 066038
[12] Q. M. Hu *et al* 2012 *Nucl. Fusion* 52 083011
[13] Q. M. Hu *et al* 2016 *Nucl. Fusion* 56 034001
[14] D. A. Maurer *et al* 2012 *Phys. Plasmas* 19 056123
[15] D. Shiraki *et al* 2013 *Phys. Plasmas* 20 102503
[16] G. Kim *et al* 2018 *Plasma Phys. Control. Fusion* 60 035009
[17] V. Igochine *et al* 2009 *Plasma Phys. Control. Fusion* 51 055008
[18] B. Esposito *et al* 2008 *Phys. Rev. Letter* 100 045006
[19] P. R. Brunsell *et al* 2004 *Phys. Rev. Letter* 93 225001
[20] N. Wang *et al* 2014 *Nucl. Fusion* 54 064014
[21] H. H. Wang *et al* 2018 *Nucl. Fusion* 58 056024
[22] W. Jin *et al* 2013 *Plasma Phys. Control. Fusion* 55 035010
[23] Y. Ding *et al* 2018 *Plasma Sci. Technol* 20 125101
[24] Y. Liang *et al* 2019 *Nucl. Fusion* 59 112016
[25] N. Wang *et al* 2022 *Nucl. Fusion* **62** 042016
[26] B. Rao *et al* 2014 *Fusion Engineering and Design* 89 378
[27] Y. Ding *et al* 2018 *Plasma Sci. Technol.* 20125101
[28] D. Guo *et al* 2017 *Rev. Sci. Instrum.* 88 123502
[29] D. L. Han *et al* 2021 *Plasma Sci. Technol.* 23 055104
[30] Z. J. Yang *et al* 2016 *Rev. Sci. Instrum*. 87 11E112
[31] L. Bardóczi *et al* 2021 *Phys. Rev. Letter* 127 055002
[32] R. Fitzpatrick *et al* 1993 *Nucl. Fusion* 33 1049
[33] D. Li *et al* Understanding the spectrum during the tearing mode locking by rotating RMP in J-

TEXT, *AIP advances*, submitted
[34] A. Gude *et al* 2021 *Plasma Phys. Control. Fusion* 63 045018
[35] Z. Huang *et al* 2020 *Nucl. Fusion* 60 064003
[36] F. Y. Mao *et al* 2022 *Plasma Sci. Technol.* 24 124002
[37] Z. K. Ren *et al* 2022 *Plasma Sci. Technol.* https://doi.org/10.1088/2058-6272/aca45f